arXiv:1209.4363v1 [cond-mat.quant-gas] 19 Sep 2012

Dynamic stabilization of a quantum many-body system

T.M. Hoang, C.S. Gerving, B.J. Land, M. Anquez, C.D. Hamley, and M.S. Chapman
School of Physics, Georgia Institute of Technology, Atlanta, GA 30332-0430

(Dated: September 21, 2012)

We demonstrate dynamic stabilization of an unstable strongly interacting quantum many-body system by periodic manipulation of the phase of the collective states. The experiment employs a spin-1 atomic Bose condensate initialized to an unstable (hyperbolic) fixed point of the spin-nematic phase space, where subsequent free evolution gives rise to squeezing and quantum spin mixing. To stabilize the system, periodic microwave pulses are applied that manipulate the spin-nematic many-body fluctuations and limit their growth. The range of pulse periods and phase shifts for which the condensate can be stabilized is measured and the resulting stability diagram compares well with a linear stability analysis of the problem.

It is well-known that unstable equilibria of physical systems can be dynamically stabilized by external periodic forcing [1]. The inverted pendulum stabilized by vertically vibrating the pivot point ('Kapitza's pendulum') provides a classic example of this non-intuitive phenomenon and was first demonstrated over 100 years ago [2, 3]. Dynamical stabilization has a broad range of applications including rf Paul traps and mass spectrometers [4], particle synchrotrons [5], and optical resonators [6]. Standard analysis of the pendulum problem [7] begins with the linearized equation of motion $\ddot{y} = (\alpha + \beta(t))y$, where y is the angular deviation from the vertical orientation, $\alpha > 0$, and $\beta(t)$ is the periodic forcing term. For $\beta = 0$, the linearized equation corresponds to an inverted harmonic oscillator, and the perfectly inverted position $y = \dot{y} = 0$ is an unstable (hyperbolic) fixed point characterized by exponentially diverging and converging orbits in phase space. For $\beta \neq 0$, determining the stability condition is a straight-forward problem of linear stability analysis. The case of harmonic forcing, $\beta(t) = \beta\cos(\omega t)$ at frequency ω yields the well-known Mathieu equation [8], which among other things describes the motion of charged particles in Paul traps.

Recent advances in ultracold atomic physics provide opportunities to investigate unstable equilibrium phenomena of interacting quantum many-body systems featuring well-characterized and controllable Hamiltonians [9]. By changing the dimensionality of the system, tuning the interaction strength [10], or magnetically quenching a spin system [11], it is possible to study excitations across a quantum phase transition described by generalizations of the Kibble-Zurek mechanism and apparent relaxation to non-thermal steady states in a well-isolated quantum system [12]. Beyond these fundamental issues, non-equilibrium dynamics can generate squeezed states and non-Gaussian states that are potential resources for quantum enhanced measurements [13] and quantum information processing [14]. Dynamic stabilization of non-equilibrium many-body Bose-Einstein condensates (BEC) has been suggested by tuning the sign of the interaction strength [15–17] and by time-varying the trapping potential in a double well BEC [18, 19]. Here, we demonstrate dynamic stabilization of the non-equilibrium dynamics of a multi-component spinor condensate. The spin dynamics following a magnetic quench are well-described by an unstable inverted harmonic oscillator in the spin-nematic degrees of freedom [20]. The non-equilibrium dynamics are stabilized by periodic application of phase shifts to the collective states of the system. Viewed broadly, the experiment demonstrates open-loop discrete control of a many-body quantum system, and is conceptually related to spin decoupling or refocusing techniques used in nuclear magnetic resonance (NMR) [21], bang-bang control of non-interacting two-level quantum systems (qubits) in quantum information processing [22] and the quantum Zeno effect [23–29]. This work paves the way for control of non-equilibrium many-body systems via direct manipulations of the quantum fluctuations.

Experimental concept

The experiment uses small spin-1 rubidium-87 condensates containing just a single domain, such that the dynamic evolution occurs only in the internal spin degrees of freedom. Within this limit, the spinor order parameter of the condensate can be written as $\psi = (\zeta_{+1}, \zeta_0, \zeta_{-1})^T$ where $\zeta_i = \sqrt{\rho_i}e^{i\theta_i}$, and $\rho_i = |\zeta_i|^2$ are the fractional populations of the three Zeeman states of the $f = 1$ ^{87}Rb ground state hyperfine manifold. The symmetry of the spin and magnetic field interactions conserves the condensate magnetization $m = (\rho_1 - \rho_{-1})$ and constrains the populations $\rho_{\pm1} = (1 - \rho_0 \pm m)/2$. For the $m = 0$ case that is relevant for these experiments, the spin dynamics are determined by the Hamiltonian [30]:

$$\mathcal{H} = \frac{c}{4}[x^2 - (1 - x^2)\cos\theta_s] + \frac{q}{2}(1 - x) \qquad (1)$$

with $x \equiv 2\rho_0 - 1$ and $\theta_s \equiv \theta_{+1} + \theta_{-1} - 2\theta_0$. The strength of the spin interaction and quadratic Zeeman energy are characterized by c and q, respectively, and $c < 0$ for ferromagnetic ^{87}Rb. This Hamiltonian has the form of a classical non-rigid pendulum and is similar to that for the double-well Bose-Hubbard model [30, 31]. The condensate has an unstable equilibrium point at $x = 1$ for small quadratic Zeeman energies and undergoes a quantum phase transition at $q = 2|c|$. The nature of the instability is more clearly revealed in the spin-nematic phase space of the Cartesian components of the spin

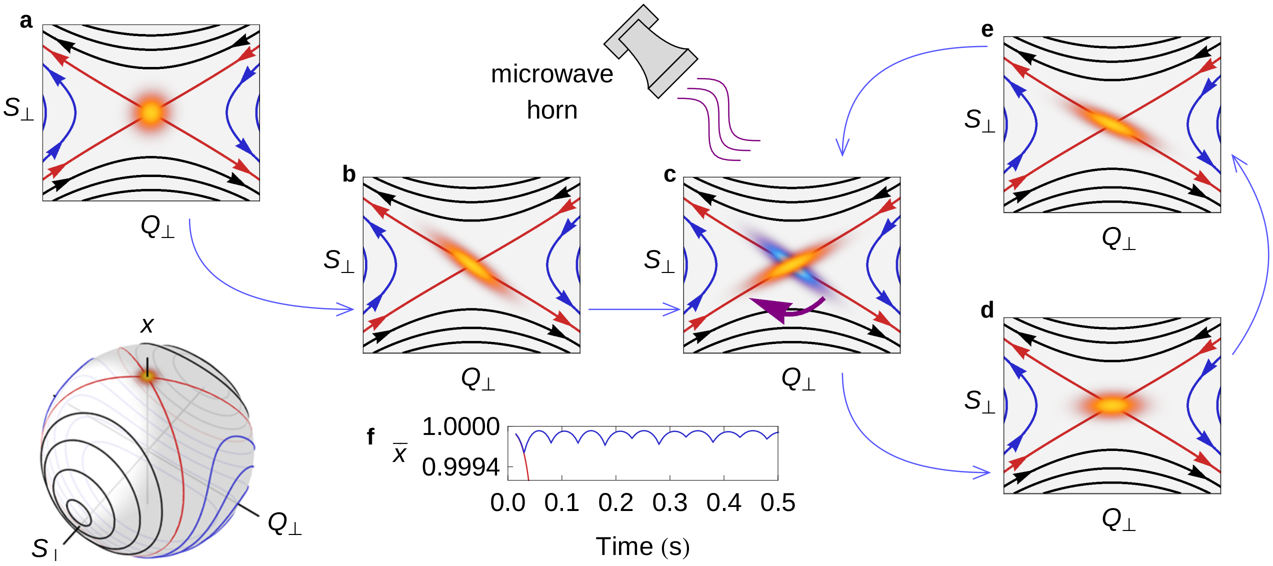

FIG. 1: **Illustration of the dynamic stabilization method.** (a) The condensate is initialized at the pole of the spin-nematic Bloch sphere, $x = 1, S_\perp = Q_\perp = 0$. The condensate has Heisenberg-limited uncertainties in $S_\perp$ and $Q_\perp$. (b) Initial free evolution of the condensate produces spin-nematic squeezing along the diverging manifold of the separatrix. (c) The quantum state of the condensate is quickly rotated to the converging manifold of the separatrix using a microwave pulse. (d) Subsequent free evolution unsqueezes the condensate, returning it close to the original state. (e) Continued free evolution again generates spin-nematic squeezing. (f) Long term stabilization is achieved by repeating the (c,d,e) sequence (blue line) whereas the unstabilized condensate rapidly evolves away (red line).

vector S_i and nematic (quadrupole) tensor Q_{ij} [32]. In this space, the spin dynamics are represented on a Bloch sphere with axes $\{S_\perp, Q_\perp, x\}$ where $S_\perp^2 = S_x^2 + S_y^2$ and $Q_\perp^2 = Q_{xz}^2 + Q_{yz}^2$. This sphere is shown in Fig. 1(a) together with the dynamical orbits of the system for $q < 2|c|$. The unstable fixed point is located at the pole of the sphere at the intersection of the two manifolds of the separatrix that divide the space into phase-winding and oscillatory phase orbits. In the neighborhood of the pole ($x \approx 1$), the Hamiltonian can be written:

$$\mathcal{H}' = \frac{q}{4} Q_\perp^2 + \frac{(q - 2|c|)}{4} S_\perp^2, \qquad (2)$$

with corresponding canonical equations of motion: $\dot{S}_\perp = q Q_\perp$ and $\dot{Q}_\perp = (2|c| - q)\, S_\perp$. These can be combined into $\ddot{Q}_\perp = \left(2|c|q - q^2\right) Q_\perp$, which, for $q < 2|c|$, describes an inverted harmonic oscillator that is inherently unstable.

The experiment uses a condensate initialized with the atoms in the $f = 1, m_f = 0$ state that corresponds to a coherent state centered at the pole of the Bloch sphere ($x = 1, S_\perp = Q_\perp = 0$) as shown in Fig. 1 (a). Evolution from this state generates Gaussian squeezed states at early times (localized near the pole) [32] and a rich variety of non-Gaussian states at later times as the system evolves on the full Bloch sphere [20]. The evolution from the initial state is driven by quantum fluctuations, $\Delta S_\perp = \Delta Q_\perp = N^{-1/2}$, where N is the number of atoms in the condensate. These fluctuations are depicted in the figure as a Husimi-Q distribution. Initial evolution in the neighborhood of the hyperbolic fixed point reduces the fluctuations along the converging manifold of the separatrix and grows the fluctuations along the diverging manifold of the separatrix; together, these create squeezing in the spin-nematic phase space.

The continued growth of the quantum correlations eventually destabilize the system and lead to evolution away from the fixed point [20]. Dynamic stabilization can be achieved by preventing the build-up of these correlations. In our experiment, this is accomplished using periodic phase shifts of the spinor order parameter that manifest as a rotation in the $S_\perp, Q_\perp$ plane about the origin. The concept is illustrated in Fig. 1 (a-d). During the initial evolution to a squeezed state, the squeezed uncertainty ellipse aligns along the diverging manifold of the separatrix. In order to prevent further growth of the correlations, the state is quickly rotated to the converging separatrix using a microwave pulse. Further evolution 'unsqueezes' the condensate and returns it approximately to the initial state, thereby stabilizing the system. Long-term stabilization is realized by periodic repetition of this cycle. Although we discuss the technique using a rotation

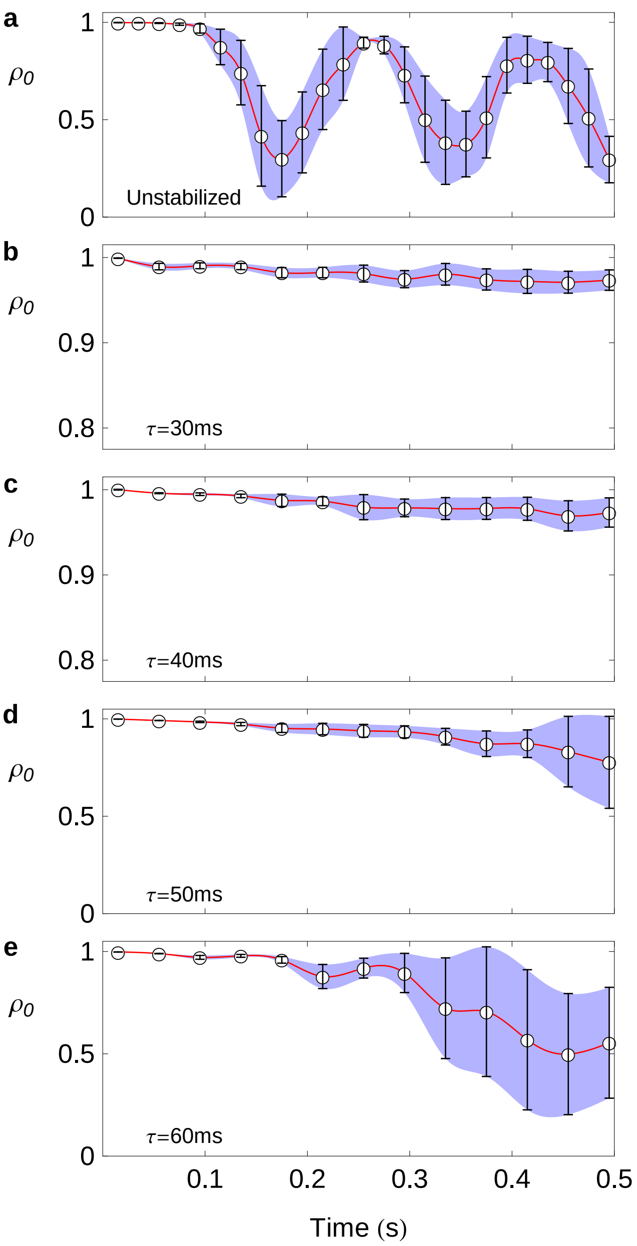

FIG. 2: **Experimental demonstration of dynamic stabilization of spin dynamics.** (a) Free (unstabilized) evolution of the spin population, ρ_0, due to quantum spin mixing ($\rho_0 = (x+1)/2$). (b)-(e) Stabilization of the spin dynamics to the $\rho_0 = 1$ unstable equilibrium using periodic rotations of the spin-nematic quadrature phase with the periods indicated. In each case, microwave pulses are used to rotate the quadrature phase through an amount $\Delta\theta = -\frac{3}{4}\pi$ rad. The open circles correspond to the mean measured value and error bars indicate the measured standard deviation. The red line and blue shaded region are smoothed interpolations to guide the eye. Note the reduced vertical scale in (b) and (c).

angle corresponding to the angles between the manifolds of the separatrix, the condensate can be stabilized for a range of angles as will be shown.

Observation of dynamic stabilization

The experiment begins with a condensate containing $N = 32,000$ atoms initialized in the $|f = 1, m_f = 0\rangle$ hyperfine state held in a high magnetic field (2 G). To initiate spin dynamics, the condensate is rapidly quenched below the quantum critical point by lowering the magnetic field to 210 mG. In order to stabilize the dynamics, the $\{S_\perp, Q_\perp\}$ quadrature phase is periodically rotated by an angle $\Delta\theta$ with a period τ. The rotation is implemented using 2π pulses on the $|f = 1, m_f = 0\rangle \leftrightarrow |f = 2, m_f = 0\rangle$ clock transition that effectively shift the phase of the $|f = 1, m_f = 0\rangle$ spinor component by an amount $\Delta\theta_0 = \pi\left(1 + \Delta/\sqrt{1+\Delta^2}\right)$ where $\Delta = \delta/\Omega$ is the detuning normalized to the on-resonance Rabi rate [32]. This pulse effects a quadrature rotation $\Delta\theta = -\Delta\theta_0$. Finally, the spin populations of the condensate are measured by imaging the condensate following expansion in a Stern-Gerlach magnetic field gradient to separate the m_f spin components. The atoms are probed for 100 μs by three pairs of orthogonal laser beams, and the fluorescence signal is collected by a CCD camera.

The experimental results demonstrating dynamic stabilization of the condensate are shown in Fig. 2 for several different pulse periods and are compared with unstabilized free evolution of the spin dynamics. The evolution of the unstabilized condensate exhibits a long initial pause (∼100 ms) in the evolution of $\langle\rho_0\rangle$ (during which spin-nematic squeezing is generated) followed by large amplitude oscillations that are characteristic of a pendulum initialized close to the unstable point. The results for the stabilization are shown for pulse periods ranging from 30–60 ms; in each case, the microwave pulse induces a quadrature rotation of $-\frac{3}{4}\pi$ rad in the $S_\perp, Q_\perp$ plane that is close to the angle between manifolds of the separatrix. The data show that the stabilization is close to perfect for pulse periods <40 ms for evolution times out to 0.5 s. For longer pulse periods, the stabilization is still effective for some time, but then eventually degrades.

In Fig. 3, the measurement of the evolution of the transverse spin fluctuations, $\Delta S_\perp$ is shown for different pulse periods. To measure $S_\perp$, a resonant RF pulse is applied to the $f = 1$ manifold to rotate $S_\perp$ into S_z before the trap is turned off. With no stabilization, the fluctuations grow exponentially, because $S_\perp$ is not aligned to the minimum quadrature squeezing angle, which is approximately the converging manifold of the separatrix. When the condensate is stabilized, the calculations show that fluctuations of $S_\perp$ first increase then decrease during each pulse cycle, which reflects the squeezing and unsqueezing of the condensate. The data show the expected periodic evolution of the fluctuations and also show a significant reduction of the fluctuations compared with the unstabilized condensate. However, the overall level of the measured fluctuations are higher than predicted, likely due to atom loss induced by the microwave pulses.

In Fig. 4, we show that the condensate spin dynam-

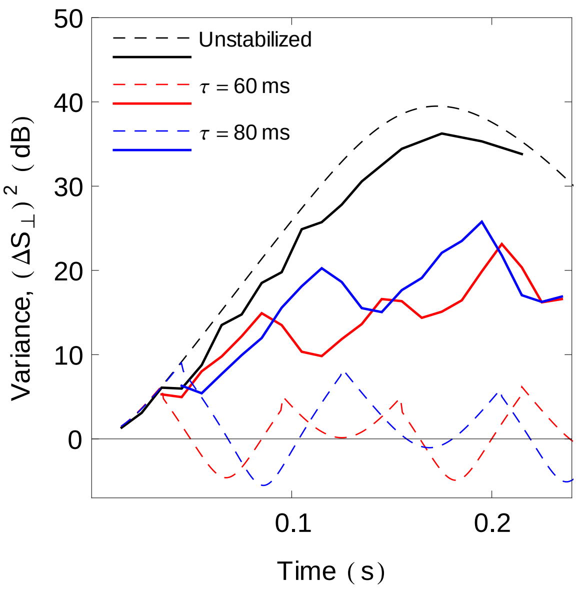

FIG. 3: **Transverse magnetization.** The fluctuations of the transverse magnetization, $S_\perp$, are measured (solid lines) for both free evolution of the condensate and for the dynamically stabilized dynamics for two different pulse periods. The results are compared to a theoretical calculations (dashed lines). The 0 dB line corresponds to the $N^{-1/2}$ standard quantum limit.

ics can be stabilized for time scales comparable and even longer than the $1/e$ lifetime of the condensate. The lifetime of the stabilized condensate is ∼500 ms, which is reduced from the 1.2 s lifetime measured without the microwave pulses. The shorter lifetime is possibly due to imperfections in the microwave Rabi pulses used to phase shift the condensate that leave some population in the $f = 2$ state, which is short-lived in the trap. The stabilization works quite robustly, despite this additional loss. We have performed two additional checks to verify that the loss does not significantly affect the dynamics of the system. In the first, we have studied the evolution of the condensate under periodic pulses with $\Delta\theta = \pi$ (the periodicity of the phase space) and verified that the condensate undergoes normal spin mixing. In the second, we have turned the stabilization pulses off after 500 ms and verified that the system again undergoes normal spin mixing.

Determining the stability region

We now turn to an investigation of the stability diagram for the condensate. Although it is conceptually simplest to understand the stabilization in terms of periodic evolutions along manifolds of the separatrix of the phase space, the condensate can be stabilized with a range of phase shifts and periods $(\Delta\theta, \tau)$. The range of stability is measured for quadrature phase rotations $\Delta\theta \in [-\pi, 0]$ and microwave pulse period τ from 5 ms to 100 ms. For each combination of $(\Delta\theta, \tau)$, the spin population is measured after 195 ms of evolution, where the unstabilized condensate shows the maximum spin-mixing (see Fig. 2). The results of the measurement are shown in Fig. 5, where each measurement point is the average of three experimental runs. For shorter period pulses, the condensate is stabilized with a wide range of quadrature phase shifts. For long period microwave pulses, the range of quadrature phase shift capable of stabilizing the dynamics shrinks and reaches an asymptotic value close to the angle between the separatrices, $\Delta\theta = \cos^{-1}(-1 - \frac{q}{c})$.

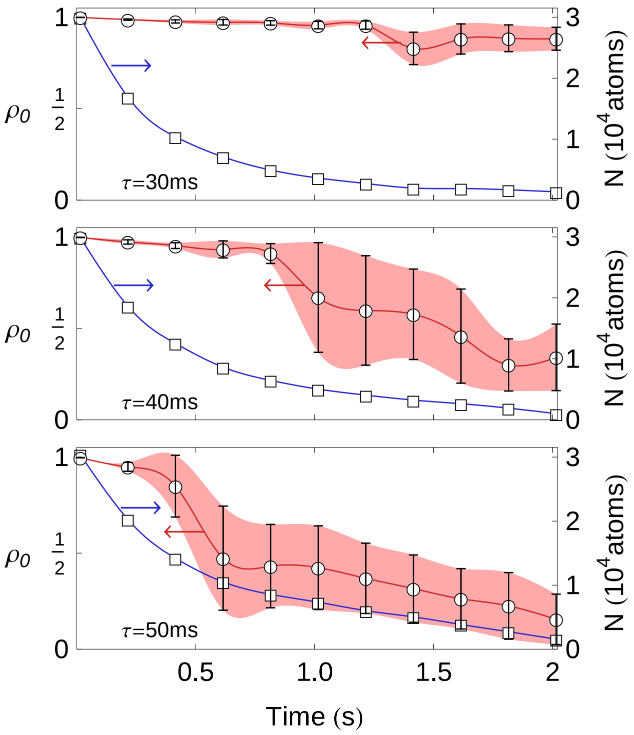

FIG. 4: **Long time stabilization dynamics of the BEC condensate.** The fractional population, ρ_0, (red, left) is compared to the total population of the condensate (blue, right). The evolution of the condensate is stabilized for periods much longer than the condensate lifetime of ∼ 500 ms.

The results are compared with a theoretical stability analysis shown in solid lines. Defining the state vector of the system $\mathbf{y} = (S_\perp, Q_\perp)^T$, the evolution of a full stabilization cycle can be written in matrix form as $\mathbf{M} = \mathbf{R}[\Delta\theta] \cdot \exp[\mathbf{m}\tau]$. $\mathbf{R}$ is the matrix for a rotation about the origin in the $S_\perp, Q_\perp$ plane, and $\Delta\theta = \Delta\theta_s/2$ is the amount of the quadrature phase shift induced by the microwave pulse. $\mathbf{m}$ is the matrix form of the equations of motion ($\dot{\mathbf{y}} = \mathbf{m}\mathbf{y}$), and τ is the period between pulses. The stability condition such that $(S_\perp, Q_\perp)$ stays bounded to the origin is $|\mathrm{Tr}[\mathbf{M}]| < 2$, which is shown as solid lines in the figure. The green lines show the stability envelope using the measured values for the spinor dynamical rate $c = -6.5(5) \times 2\pi$ Hz and the magnetic

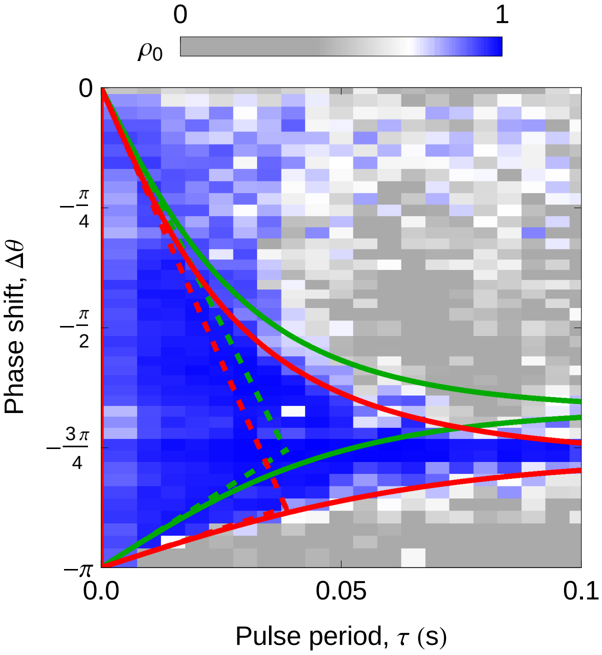

FIG. 5: **Stability diagram.** To map the stability region, the mean ρ_0 is measured at the time of the maximum spin mixing for the unstabilized condensate. The solid curves are the envelope of the calculated stability region using linear stability analysis, while the dashed curves use a time-averaged Hamiltonian approach. The green curves use the measured values $B = 210$ mG, $c = -6.5 \times 2\pi$ Hz, and the red curves use $B_{\text{eff}} = 150$ mG, $c = -6.5 \times 2\pi$ Hz.

field $B = 210(10)$ mG that determines the quadratic Zeeman effect $q = 71.6 \times B^2$ Hz/G^2. Although the measured stability region is in good qualitative agreement with the theoretical envelope, there is an offset in the asymptotic phase for long periods between experimental and theory which is about 0.3 rad. This discrepancy is larger than can be accounted for in the uncertainties of the determination of c and q, the former determined by direct measurement of coherent spinor oscillations of the condensate, and the latter determined by RF and microwave spectroscopy on magnetic field sensitive hyperfine transitions. Using a magnetic field value of $B_{\text{eff}} = 150$ mG for the theoretical calculation provides a much better agreement with the data, as is indicated by the red solid lines. We suspect that small differential AC stark shifts of the Zeeman states induced by the 850 nm optical trap beam (at the level of a few Hz) are responsible for this discrepancy. The measurements also seem to indicate that the system exhibits stability outside the analytical envelope for small phase shifts, $\Delta\theta > -\pi/4$. This is an artifact of the fact that the measurement is determined at a relatively early time (195 ms), where, for small applied phase shifts, the evolution of the condensate is similar to the freely evolving case with smaller amplitude spin-mixing oscillations and large non-Gaussian fluctuations.

It is also possible to derive a stability diagram using a time-averaged effective Hamiltonian method. For $c < 0$, the $m_f = 0$ state is stable if the quadratic Zeeman energy is greater than $2|c|$ or less than zero. For the applied phase shifts using the periodic microwave pulses we can calculate an effective quadratic Zeeman energy, $q_{\text{eff}} = q + \hbar\Delta\theta/\tau$. Due to the cyclic nature of the phase space, the quadrature shift pulse can be interpreted as a positive or negative pulse. Because of this ambiguity of the phase shift direction, q_{eff} is double valued everywhere. For both $q_{\text{eff}} > 2|c|$ and $q_{\text{eff}} < 0$ there is no longer a hyperbolic fixed point centered on the pure $m_f = 0$ state, and hence wherever these conditions are met for both of the q_{eff} values, the system should be stable. The stability boundaries determined using this approach are shown by the dashed lines in Fig. 5. They are more restrictive than the linear stability analysis, although they agree asymptotically for shorter pulse periods.

Conclusion and outlook

These experiments demonstrate new methods of manipulating out-of-equilibrium quantum many-body systems, drawing together ideas from classical Hamiltonian dynamics and quantum squeezing of collective states. In future work, it should be possible to engineer highly entangled states of the system (including Schrödinger cat-like states) using extensions of these ideas [33] and to demonstrate other fundamental phenomena such as Berry phases [34].

---

[1] L.D. Landau and E.M. Lifshitz. *Mechanics*. Course of theoretical physics. Butterworth-Heinemann, 1976.

[2] Andrew Stepheson. On induced stability. *Philosophical Magazine*, 15:233–236, 1908.

[3] Pyotr Leonidovich Kapitza. Dynamic stability of a pendulum when its point of suspension vibrates. *Soviet Phys. JETP*, 21:588–592, 1951.

[4] Wolfgang Paul. Electromagnetic traps for charged and neutral particles. *Rev. Mod. Phys.*, 62:531–540, Jul 1990.

[5] Ernest D. Courant, M. Stanley Livingston, and Hartland S. Snyder. The strong-focusing synchroton¯a new high energy accelerator. *Phys. Rev.*, 88:1190–1196, Dec 1952.

[6] A.E. Siegman. *Lasers*. University Science Books, 1986.

[7] Eugene I. Butikov. On the dynamic stabilization of an inverted pendulum. *American Journal of Physics*, 69(7):755–768, 2001.

[8] N. W. McLachlan. *Theory and Applications of Mathieu Functions*. Oxford University Press, Oxford, 1947.

[9] Immanuel Bloch, Jean Dalibard, and Wilhelm Zwerger. Many-body physics with ultracold gases. *Rev. Mod. Phys.*, 80:885–964, Jul 2008.

[10] Cheng Chin, Rudolf Grimm, Paul Julienne, and Eite Tiesinga. Feshbach resonances in ultracold gases. *Rev. Mod. Phys.*, 82:1225–1286, Apr 2010.

[11] D.M. Stamper-Kurn and M. Ueda. Spinor bose gases: Explorations of symmetries, magnetism and quantum dynamics. arXiv:1205.1888 [cond-mat.quant-gas], to appear.

[12] Anatoli Polkovnikov, Krishnendu Sengupta, Alessandro Silva, and Mukund Vengalattore. Nonequilibrium dynamics of closed interacting quantum systems. *Rev. Mod. Phys.*, 83:863–883, 2011.

[13] J. Ma, X.G. Wang, C.P. Sun, and F. Nori. Quantum spin squeezing. *PHYSICS REPORTS*, 509, 2011.

[14] Samuel L. Braunstein and Peter van Loock. Quantum information with continuous variables. *Rev. Mod. Phys.*, 77:513–577, Jun 2005.

[15] Hiroki Saito and Masahito Ueda. Dynamically stabilized bright solitons in a two-dimensional bose-einstein condensate. *Phys. Rev. Lett.*, 90:040403, Jan 2003.

[16] Hiroki Saito, Randall G. Hulet, and Masahito Ueda. Stabilization of a bose-einstein droplet by hyperfine rabi oscillations. *Phys. Rev. A*, 76:053619, Nov 2007.

[17] R.L. Compton, Y.-J. Lin, K. Jimenez-Garcia, J.V. Porto, and I.B. Spielman. Dynamically slowed collapse of a bose-einstein condensate with negative scattering length. *ArXiv e-prints*, Jul 2012.

[18] Erez Boukobza, Michael G. Moore, Doron Cohen, and Amichay Vardi. Nonlinear phase dynamics in a driven bosonic josephson junction. *Phys. Rev. Lett.*, 104:240402, Jun 2010.

[19] F. Sols and S. Kohler. Shapiro resonances in an isolated ac-driven double bose-einstein condensate. *Laser Physics*, 14:1259–1264, September 2004.

[20] C.S. Gerving, T.M. Hoang, B. Land, M. Anquez, C. D. Hamley, and M. S. Chapman. Non-equilibrium dynamics of an unstable quantum pendulum. arXiv:1205.2121 [cond-mat.quant-gas], to appear.

[21] R.R. Ernst, G. Bodenhausen, and A. Wokaun. *Principles of Nuclear Magnetic Resonance in One and Two Dimensions*. Clarendon Press, Oxford, 1987.

[22] Lorenza Viola and Seth Lloyd. Dynamical suppression of decoherence in two-state quantum systems. *Phys. Rev. A*, 58:2733–2744, Oct 1998.

[23] P. Facchi, D. A. Lidar, and S. Pascazio. Unification of dynamical decoupling and the quantum zeno effect. *Phys. Rev. A*, 69:032314, Mar 2004.

[24] B. Misra and E. C. G. Sudarshan. The zeno's paradox in quantum theory. *Journal of Mathematical Physics*, 18(4):756–763, 1977.

[25] Wayne M. Itano, D. J. Heinzen, J. J. Bollinger, and D. J. Wineland. Quantum zeno effect. *Phys. Rev. A*, 41:2295–2300, Mar 1990.

[26] M. C. Fischer, B. Gutiérrez-Medina, and M. G. Raizen. Observation of the quantum zeno and anti-zeno effects in an unstable system. *Phys. Rev. Lett.*, 87:040402, Jul 2001.

[27] Erik W. Streed, Jongchul Mun, Micah Boyd, Gretchen K. Campbell, Patrick Medley, Wolfgang Ketterle, and David E. Pritchard. Continuous and pulsed quantum zeno effect. *Phys. Rev. Lett.*, 97:260402, Dec 2006.

[28] J. Bernu, S. Deléglise, C. Sayrin, S. Kuhr, I. Dotsenko, M. Brune, J. M. Raimond, and S. Haroche. Freezing coherent field growth in a cavity by the quantum zeno effect. *Phys. Rev. Lett.*, 101:180402, Oct 2008.

[29] Simon Gustavsson, Fei Yan, Jonas Bylander, Fumiki Yoshihara, Yasunobu Nakamura, Terry P. Orlando, and William D. Oliver. Dynamical decoupling and dephasing in interacting two-level systems. *Phys. Rev. Lett.*, 109:010502, Jul 2012.

[30] W. Zhang, D. L. Zhou, M.-S. Chang, M. S. Chapman, and L. You. Coherent spin mixing dynamics in a spin-1 atomic condensate. *Phys. Rev. A*, 72(1):013602, 2005.

[31] A. Smerzi, S. Fantoni, S. Giovanazzi, and S. R. Shenoy. Quantum coherent atomic tunneling between two trapped bose-einstein condensates. *Phys. Rev. Lett.*, 79:4950–4953, 1997.

[32] C. D. Hamley, C.S. Gerving, T.M. Hoang, E. M. Bookjans, and M. S. Chapman. Spin-nematic squeezed vacuum in a quantum gas. *Nature Phys.*, 8:305–308, 2012.

[33] William P. Reinhardt. Mary Ann Leung, Khan W. Mahmud. Dynamical studies of macroscopic superposition states: Phase engineering of controlled entangled number states of bose-einstein condensate in multiple wells. arXiv:1006.2556v2 [cond-mat.quant-gas].

[34] S. C. Li, J. Liu, and L. B. Fu. Berry phase and hannay angle of an interacting boson system. *Phys. Rev. A*, 83:042107, Apr 2011.

arXiv:1209.4363v1 [cond-mat.quant-gas] 19 Sep 2012

Dynamic Stabilization of a Quantum Many-body System: Supplementary Information

T.M. Hoang, C.S. Gerving, B.J. Land, M. Anquez, C.D. Hamley, and M.S. Chapman
School of Physics, Georgia Institute of Technology, Atlanta, GA 30332-0430

(Dated: September 21, 2012)

In this Supplementary Information, we derive the stability regions shown in the main paper for pulsed quadrature phase shifts applied periodically during the evolution. The derivation follows standard methods of stability analysis for step-wise evolution used for example in optical resonator stability analysis. We compare this method with an analysis based on the time-average of the Hamiltonian that provides more restrictive condition in disagreement with the experiment.

I. SEMI-CLASSICAL EQUATIONS

Within the single mode approximation (in which the spin states share a common spatial wavefunction), the mean-field order parameter is represented by a complex vector $(\zeta_1, \zeta_0, \zeta_{-1})^T$ where ζ_i represents the amplitude and phase of the classical field for the mode associated with the m_f state given in the index. A mean field analysis of the spin Hamiltonian [1–3] produces the dynamical equations [4]:

$$\begin{aligned} i\hbar\dot{\zeta}_1 &= E_1\zeta_1 + c[(\rho_1+\rho_0-\rho_{-1})\zeta_1 + \zeta_0^2\zeta_{-1}^*] \\ i\hbar\dot{\zeta}_0 &= E_0\zeta_0 + c[(\rho_1+\rho_{-1})\zeta_0 + 2\zeta_1\zeta_{-1}\zeta_0^*] \\ i\hbar\dot{\zeta}_{-1} &= E_{-1}\zeta_{-1} + c[(\rho_{-1}+\rho_0-\rho_1)\zeta_{-1} + \zeta_0^2\zeta_1^*] \end{aligned}$$

where c is the spin interaction energy, $\rho_i \equiv N_i/N = |\zeta_i|^2$ is the fractional population of the $m_f = i$ component, and E_i is the magnetic field energy for each mode.

A convenient parameterization of the order parameter is given by

$$\begin{aligned} \zeta_1 &= \sqrt{\frac{1-\rho_0+m}{2}}e^{i\frac{\theta_s+\theta_m}{2}} \\ \zeta_0 &= \sqrt{\rho_0} \\ \zeta_{-1} &= \sqrt{\frac{1-\rho_0-m}{2}}e^{i\frac{\theta_s-\theta_m}{2}} \end{aligned} \tag{1}$$

where $\theta_m = \theta_1 - \theta_{-1}$ is the magnetization or Larmor precession phase, $\theta_s = \theta_1 + \theta_{-1} - 2\theta_0$ is the spinor phase, and $m = (N_1 - N_{-1})/N = \rho_1 - \rho_{-1}$ is the fractional magnetization, which is a constant of the motion.

Using this parameterization, the dynamical equations reduce to [5]:

$$\begin{aligned} \dot{\rho}_0 &= \frac{2c}{\hbar}\rho_0\sqrt{(1-\rho_0)^2-m^2}\sin\theta_s \\ \dot{\theta}_s &= -\frac{2q}{\hbar} + \frac{2c}{\hbar} \times \\ &\quad \left[(1-2\rho_0) + \frac{(1-\rho_0)(1-2\rho_0)-m^2}{\sqrt{(1-\rho_0)^2-m^2}}\cos\theta_s\right]. \end{aligned}$$

ρ_0 and θ_s are canonically conjugate variables and the dynamical phase space is defined by the corresponding spin energy functional of the condensate:

$$\begin{aligned} \mathcal{E} &= \frac{c}{2}m^2 + c\rho_0\left[(1-\rho_0) + \sqrt{(1-\rho_0)^2-m^2}\cos\theta_s\right] \\ &\quad + pm + q(1-\rho_0). \end{aligned} \tag{2}$$

m and θ_m are also canonically conjugate variables. However, θ_m is cyclic because it does not appear in the energy functional, and thus m is conserved.

II. DYNAMICAL ANALYSIS

The first step is to recast the energy functional Eqn. 2 in terms of the spin and nemantic operators. We will restrict ourselves to the $m = 0$ case which is relevant for the experiments. In this case, Eqn. 2 becomes:

$$\mathcal{E} = c\rho_0(1-\rho_0)(1+\cos\theta_s) + q(1-\rho_0).$$

Substituting $x = 2\rho_0 - 1$ gives

$$\mathcal{E} = \frac{c}{4}\left(1-x^2\right)(1+\cos\theta_s) + \frac{q}{2}(1-x)$$

which is the same as Eqn. 1 of the main paper up to constants.

Next, we evaluate the expectation values of the several of the mean field spin and quadrupole operators (provided in Appendix) using the parameterization for the order parameter in Eqn. 1 with $m = 0$,

$$\begin{aligned} \langle S_x\rangle &= 2\sqrt{\rho_0(1-\rho_0)}\cos\frac{\theta_s}{2}\cos\frac{\theta_m}{2} \\ \langle Q_{yz}\rangle &= 2\sqrt{\rho_0(1-\rho_0)}\sin\frac{\theta_s}{2}\cos\frac{\theta_m}{2} \\ \langle S_y\rangle &= -2\sqrt{\rho_0(1-\rho_0)}\cos\frac{\theta_s}{2}\sin\frac{\theta_m}{2} \\ \langle Q_{xz}\rangle &= -2\sqrt{\rho_0(1-\rho_0)}\sin\frac{\theta_s}{2}\sin\frac{\theta_m}{2}. \end{aligned}$$

Note that for the mean field all of these quadrature values range from -1 to 1. From these we calculate the relationships

$$\begin{aligned} S_\perp^2 &= S_x^2 + S_y^2 = 4\rho_0\left(1-\rho_0\right)\cos^2\frac{\theta_s}{2} \\ &= 2\rho_0\left(1-\rho_0\right)\left(1+\cos\theta_s\right) \\ &= \frac{1}{2}\left(1-x^2\right)\left(1+\cos\theta_s\right) \end{aligned}$$

$$\begin{aligned} Q_\perp^2 &= Q_{xz}^2 + Q_{yz}^2 = 4\rho_0\left(1-\rho_0\right)\sin^2\frac{\theta_s}{2} \\ &= 2\rho_0\left(1-\rho_0\right)\left(1-\cos\theta_s\right) \\ &= \frac{1}{2}\left(1-x^2\right)\left(1-\cos\theta_s\right) \end{aligned}$$

$$S_\perp^2 + Q_\perp^2 + x^2 = 1.$$

Substituting these relationships back into the energy functional gives

$$\mathcal{E} = \frac{c}{2}S_\perp^2 + \frac{q}{2(1+x)}\left(S_\perp^2 + Q_\perp^2\right).$$

For low depeletion $x \rightarrow 1$ corresponding to the top of the Bloch sphere, we can write the following approximation:

$$\mathcal{E} = \frac{q}{4}Q_\perp^2 + \left(\frac{q}{4}+\frac{c}{2}\right)S_\perp^2. \tag{3}$$

For the $f = 1$ ^{87}Rb condensates, $c < 0$, and so for large positive values of q, the system is isomorphic to a stable harmonic oscillator, while for small q, the system is isomorphic to an unstable ('inverted') harmonic oscillator. The cross-over point at $q = 2|c|$ is a quantum phase transition.

III. STABILITY CONDITION

From Eqn. 3, the canonical equations of motion are derived as follows

$$\begin{aligned} \dot{S}_\perp &= \frac{2}{\hbar}\frac{\partial\mathcal{E}}{\partial Q_{\perp z}} = \tilde{q}Q_{\perp z} \\ \dot{Q}_{\perp z} &= -\frac{2}{\hbar}\frac{\partial\mathcal{E}}{\partial S_\perp} = -\left(2\tilde{c}+\tilde{q}\right)S_\perp, \end{aligned}$$

where $\tilde{c} = c/\hbar$ and $\tilde{q} = q/\hbar$ are angular frequencies. This can be written in a matrix form

$$\begin{pmatrix} \dot{S}_\perp \\ \dot{Q}_{\perp z} \end{pmatrix} = \begin{pmatrix} 0 & \tilde{q} \\ -\left(2\tilde{c}+\tilde{q}\right) & 0 \end{pmatrix} \begin{pmatrix} S_\perp \\ Q_{\perp z} \end{pmatrix}$$

which is more amenable to the stability analysis to follow. Defining this matrix as $\mathbf{m}$, the full dynamics from one pulse to another including the quadrature phase shift (which is just a plane rotation in $S_\perp$ and $Q_{\perp z}$) is given by

$$\mathbf{M} = \mathbf{R}[\Delta\theta]\cdot\exp[\tau\mathbf{m}]$$

where τ is the period between pulses, $\mathbf{R}$ is a rotation matrix, and $\Delta\theta = \Delta\theta_s/2$ is the amount of the quadrature phase shift. From this point the stability condition is exactly the same as an optical resonator using ray tracing techniques. The determinant of the one pass evolution matrix must meet the condition $|\mathrm{Tr}[\mathbf{M}]| < 2$. This inequality is used to mark the boundaries of the analytic stability region, which compares favorably to simulations.

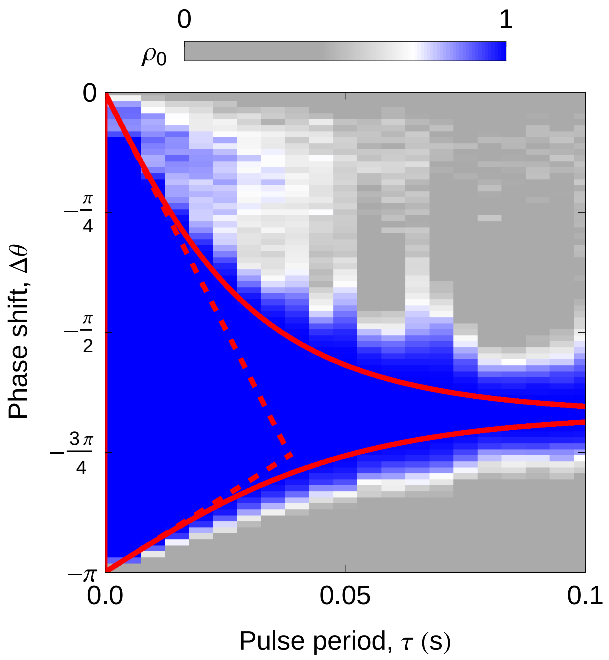

FIG. 1: **Stability mapping.** Simulation values of ρ_0 at the time of the maximum spin mixing are used to map the stability region and analytical fit

IV. EFFECTIVE QUADRATIC ZEEMAN ANALYSIS

Another way to analyze the stability is through the use of a time-averaged, effective quadratic Zeeman. For $c < 0$, it is known that the system does not evolve from the $m_f = 0$ state if the quadratic Zeeman energy is greater than $2|c|$ or less than zero. We note that the quadratic Zeeman portion of $\mathbf{m}$ is just a two dimensional rotation matrix rotating the quadratures by an angle of $q\tau/\hbar$. The microwave pulse generates an instantaneous quadrature rotation of $\Delta\theta$. Therefore over one period of the periodic microwave pulse sequence we can calculate an effective quadratic Zeeman, $q_{\text{eff}} = q + \hbar\Delta\theta/\tau$. The phase space is cyclic with a periodicity of π in quadrature phase. So an instantaneous phase shift of $\Delta\theta$ is equivalent to a phase shift of $\Delta\theta - \pi$, which is a negative contribution to q_{eff}. Because of this ambiguity of the phase shift direction, q_{eff} is double valued everywhere. Both values are needed for the time-averaged analysis of the stability. For both $q_{\text{eff}} > 2|c|$ and $q_{\text{eff}} < 0$ there is no longer a hyperbolic fixed point centered on the $m_f = 0$ state. Wherever these conditions are met for both of the q_{eff} values, then the system is trivially stable. This region is bounded by the dashed lines in the stability diagram. The dynamical solutions asymptote to these lines for short time between pulses.

Appendix: Spin and Quadrupole Operators

TABLE I: Spin-1 dipole operators. Expectation values of these operators are components of the angular momentum vector. Matrices in spherical polar basis $|f, m_f\rangle$.

$S_x = \frac{1}{\sqrt{2}} \begin{pmatrix} 0 & 1 & 0 \\ 1 & 0 & 1 \\ 0 & 1 & 0 \end{pmatrix}$	$\hat{S}_x = \frac{1}{\sqrt{2}} \left(\hat{a}_1^\dagger \hat{a}_0 + \hat{a}_0^\dagger \hat{a}_{-1} + \hat{a}_0^\dagger \hat{a}_1 + \hat{a}_{-1}^\dagger \hat{a}_0 \right)$
$S_y = \frac{i}{\sqrt{2}} \begin{pmatrix} 0 & -1 & 0 \\ 1 & 0 & -1 \\ 0 & 1 & 0 \end{pmatrix}$	$\hat{S}_y = \frac{i}{\sqrt{2}} \left(-\hat{a}_1^\dagger \hat{a}_0 - \hat{a}_0^\dagger \hat{a}_{-1} + \hat{a}_0^\dagger \hat{a}_1 + \hat{a}_{-1}^\dagger \hat{a}_0 \right)$
$S_z = \begin{pmatrix} 1 & 0 & 0 \\ 0 & 0 & 0 \\ 0 & 0 & -1 \end{pmatrix}$	$\hat{S}_z = \left(\hat{a}_1^\dagger \hat{a}_1 - \hat{a}_{-1}^\dagger \hat{a}_{-1} \right)$

TABLE II: The spin-1 quadrapole operators. Expectation values of these operators are moments of the symmetric traceless quadrapole tensor. Matrices in spherical polar basis $|f, m_f\rangle$.

$Q_{yz} = \frac{i}{\sqrt{2}} \begin{pmatrix} 0 & -1 & 0 \\ 1 & 0 & 1 \\ 0 & -1 & 0 \end{pmatrix}$	$\hat{Q}_{yz} = \frac{i}{\sqrt{2}} \left(-\hat{a}_1^\dagger \hat{a}_0 + \hat{a}_0^\dagger \hat{a}_{-1} + \hat{a}_0^\dagger \hat{a}_1 - \hat{a}_{-1}^\dagger \hat{a}_0 \right)$
$Q_{xz} = \frac{1}{\sqrt{2}} \begin{pmatrix} 0 & 1 & 0 \\ 1 & 0 & -1 \\ 0 & -1 & 0 \end{pmatrix}$	$\hat{Q}_{xz} = \frac{1}{\sqrt{2}} \left(\hat{a}_1^\dagger \hat{a}_0 - \hat{a}_0^\dagger \hat{a}_{-1} + \hat{a}_0^\dagger \hat{a}_1 - \hat{a}_{-1}^\dagger \hat{a}_0 \right)$
$Q_{xy} = i \begin{pmatrix} 0 & 0 & -1 \\ 0 & 0 & 0 \\ 1 & 0 & 0 \end{pmatrix}$	$\hat{Q}_{xy} = i \left(-\hat{a}_1^\dagger \hat{a}_{-1} + \hat{a}_{-1}^\dagger \hat{a}_1 \right)$
$Q_{xx} = \begin{pmatrix} -\frac{1}{3} & 0 & 1 \\ 0 & \frac{2}{3} & 0 \\ 1 & 0 & -\frac{1}{3} \end{pmatrix}$	$\hat{Q}_{xx} = -\frac{1}{3}\hat{a}_{+1}^\dagger \hat{a}_{+1} + \frac{2}{3}\hat{a}_0^\dagger \hat{a}_0 - \frac{1}{3}\hat{a}_{-1}^\dagger a_{-1} + \hat{a}_{+1}^\dagger \hat{a}_{-1} + \hat{a}_{-1}^\dagger \hat{a}_{+1}$
$Q_{yy} = \begin{pmatrix} -\frac{1}{3} & 0 & -1 \\ 0 & \frac{2}{3} & 0 \\ -1 & 0 & -\frac{1}{3} \end{pmatrix}$	$\hat{Q}_{yy} = -\frac{1}{3}\hat{a}_{+1}^\dagger \hat{a}_{+1} + \frac{2}{3}\hat{a}_0^\dagger \hat{a}_0 - \frac{1}{3}\hat{a}_{-1}^\dagger \hat{a}_{-1} - \hat{a}_{+1}^\dagger \hat{a}_{-1} - \hat{a}_{-1}^\dagger \hat{a}_{+1}$
$Q_{zz} = \begin{pmatrix} \frac{2}{3} & 0 & 0 \\ 0 & -\frac{4}{3} & 0 \\ 0 & 0 & \frac{2}{3} \end{pmatrix}$	$\hat{Q}_{zz} = \frac{2}{3}\hat{a}_{+1}^\dagger \hat{a}_{+1} - \frac{4}{3}\hat{a}_0^\dagger \hat{a}_0 + \frac{2}{3}\hat{a}_{-1}^\dagger \hat{a}_{-1}$

---

[1] T.-L. Ho. Spinor Bose condensates in optical traps. *Phys. Rev. Lett.*, 81:742–745, 1998.

[2] T. Ohmi and K. Machida. Bose-Einstein condensation with internal degrees of freedom in alkali atom gases. *J. Phys. Soc. Jpn*, 67:1822–1825, 1998.

[3] J. Stenger, S. Inouye, D. M. Stamper-Kurn, H.-J. Miesner, A. P. Chikkatur, and W. Ketterle. Spin domains in ground-state Bose-Einstein condensates. *Nature*, 396:345, 1999.

[4] H. Pu, C. K. Law, S. Raghavan, J. H. Eberly, and N. P.

Bigelow. Spin-mixing dynamics of a spinor Bose-Einstein condensate. *Phys. Rev. A*, 60:1463–1470, 1999.

[5] W. Zhang, D. L. Zhou, M.-S. Chang, M. S. Chapman, and L. You. Coherent spin mixing dynamics in a spin-1 atomic condensate. *Phys. Rev. A*, 72(1):013602, 2005.